Hindawi
Geofluids
Volume 2021, Article ID 1751256, 16 pages
https://doi.org/10.1155/2021/1751256

Research Article

Optical Fiber Frequency Shift Characterization of Overburden Deformation in Short-Distance Coal Seam Mining

Dingding Zhang,[1,2] **Qiang Chen**,[3] **Zhengshuai Wang**,[4] **Jianfeng Yang**,[1,2] **and Jing Chai**[1,2]

[1]*School of Energy Engineering, Xi'an University of Science and Technology, Xi'an 710054, China*
[2]*Key Laboratory of Western Mine Exploitation and Hazard Prevention, Xi'an 710054, China*
[3]*Jining No. 3 Coal Mine, Yanzhou Coal Mining Co., Ltd., Jining 272000, China*
[4]*China Coal Technology Engineering Group Chongqing Research Institute Co., Ltd., Chongqing 400037, China*

Correspondence should be addressed to Dingding Zhang; zhangdd@xust.edu.cn

Received 9 September 2021; Accepted 6 October 2021; Published 19 October 2021

Academic Editor: Yu Wang

Overburden deformation is an important concern for the safe and green mining of coal resources. Similarity simulation testing is the main approach used to study the deformation characteristics of the overburden in coal mining. In the application of Brillouin optical time-domain analysis (BOTDA) in similarity simulation tests, the capability of distributed optical fiber sensing (DOFS) to detect the characteristics of the overburden deformation and the evolution is a key factor affecting the testing accuracy. In this study, the relationships between DOFS and overburden deformation and the face impact pressure under geological conditions in short-distance coal seam mining were explored. The results show that DOFS can be used to monitor the strain conditions of the overburden during the entire mining process and can provide the peak positions of the advance support pressure on the face. A DOFS characterization model for investigating the spatial and temporal evolutions of overburden deformation was established. A new method of characterizing the face impact pressure based on the fiber frequency shift variation was developed. The method was demonstrated to be effective through comparison of monitored results of impact pressure counts detected using pressure sensors. The characteristics of the face impact pressure in short-distance coal seam mining were obtained. The results of this study provide valuable guidance for the development of similarity simulation testing and intelligent mining engineering techniques.

1. Introduction

The mining of coal resources can destroy the overburden rock layers, resulting in soil and water losses at the ground surface, damage to the regional ecological balance, and many other serious environmental problems [1–3]. Current mining techniques have evolved from shallow, single coal seam to multilayer mining. The overlying rocks are affected by repeated mining disturbances [4]. The overburden migration characteristics caused by the mining are fundamentally important to the development of mining techniques, and they are of great significance to the prevention and control of mining-related geological disasters such as rock burst, coal (rock) body protrusion, roadway deformation, and water inrush from the roof and floor [5–7]. However, the on-site in situ research has been limited by high costs, great technical difficulties, and restricted monitoring equipment [8, 9]. Therefore, similarity simulation testing is the main approach used to investigate the characteristics of the overburden deformation, fracturing, and roof impact pressure [10, 11]. At present, close-range photography, total station instruments, and dial indicators are usually used to obtain displacement measurements in similarity simulation tests, while strain gauges and pressure sensors are widely used for stress and strain monitoring. Due to the low test accuracy and disadvantages of scattered measurements only at selected locations, these testing methods are difficult to use for the continuous measurement of the entire field in real time [12, 13].

Optical fiber monitoring techniques have many advantages such as high precision, corrosion resistance, and electromagnetic interference resistance. They are widely used in monitoring the quality of structures in the electric power, mining, and construction industries [14, 15]. Among them, Brillouin optical time-domain analysis (BOTDA) is outstanding due to its high precision, distributed measurements, and the measurements of the absolute temperature and strain [16–18]. Horiguchi et al. [19] first proposed the distributed optical fiber sensor monitoring technique based on stimulated Brillouin scattering in 1989. Bao et al. [20] proposed Brillouin optical time-domain analysis with differential pulse-width pairs (DPP-BOTDA) based on a difference method in order to further improve the spatial resolution of optical fiber monitoring. Kishida et al. [21] proposed pulse-prepump Brillouin optical time-domain analysis (PPP-BOTDA) to obtain high spatial resolution and high-precision strain measurements via optical fiber sensing. Song et al. [22] proposed a new monitoring technique for distributed optical fiber sensing to achieve a centimeter-level spatial resolution.

BOTDA can be used for internal strain monitoring of rock strata, and it is an important monitoring method for detecting rock deformation [23, 24]. Moffat et al. [25] used a distributed optical fiber sensing monitoring system based on BOTDA to detect the displacement of the tunnel roof and the tunnel's two sides in order to evaluate rock deformation due to mining activities. Buchoud et al. [26] used artificial collapse pits to simulate surface collapse pits and to carry out surface subsidence displacement monitoring based on distributed optical fiber sensing (DOFS) and achieved submillimeter-level vertical surface displacement measurements. Zhang et al. [27] used inclined drilling to implant distributed sensing optical cables in the sampling field of their similarity simulation test in order to accomplish strain field monitoring of overburden deformation during mining. Chai et al. [28] applied the distributed strain fiber technique to a three-dimensional physical similarity simulation test to conduct quantitative characterization of the internal deformation and failure of mining-induced overburden.

In this study, a distributed optical fiber sensing technique (BOTDA) was applied in a physical similarity simulation test. Distributed optical fiber sensors were used to test the internal strain of the overburden under repeated mining conditions and to explore the relationships between the overburden failure, face impact pressure, and optical fiber monitoring results. The results of this study provide a useful basis for the application of distributed optical fiber sensing in similarity simulation testing in mining engineering.

2. Similarity Simulation Test Based on Distributed Optical Fiber Sensing Monitoring

2.1. Principle of PPP-BOTDA. The propagation of light in an optical fiber produces three scattering signals: Rayleigh scattering, Raman scattering, and Brillouin scattering. Brillouin scattered light is caused by nonlinear interactions between incident light and phonons that are thermally excited within the light propagation medium. This scattered light shifts in frequency by a Brillouin shift and propagates in the opposite direction relative to the incident light [29]. Figure 1 shows the monitoring principle of BOTDA.

Compared to BOTDA, PPP-BOTDA (i.e., pulse-prepump-Brillouin optical time domain analyzer) [26], higher spatial resolution can be obtained. This is done by loading an appropriate pulse-prepumped light to preexcite phonons before introducing the pulsed light (pumped light.) The PPP-BOTDA has a smaller half-value full width and higher frequency resolution of the Brillouin gain spectrum, achieving a spatial resolution of 10 mm and 0.0025% strain test accuracy.

It has been found that there is a relationship between Brillouin frequency shift (BFS) ν_B and temperature T or strain ε; the relationship can be expressed as follows [30]:

$$V_{B2} = V_{B1} + C_T(T - T_0) + C_\varepsilon \Delta\varepsilon, \tag{1}$$

where ν_{B2} is Brillouin scattered frequency shift with strain at a certain temperature T, ν_{B1} is Brillouin scattered frequency shift without strain at temperature T_0, C_T is the sensitivity coefficient of the fiber to temperature, C_ε is the sensitivity coefficient of the fiber to strain, and T_0 is the initial temperature. The C_{VT} is 1.07 MHz/°C, and the $C_{V\varepsilon}$ is 0.0497 MHz/$\mu\varepsilon$.

It is worth noting that the temperature-induced Brillouin frequency shift is much smaller than that caused by strain (0.002%/°C). Therefore, when measuring the Brillouin frequency shift caused by strain, if the temperature changes within 5°C, the temperature can be ignored.

2.2. Similarity Simulation Test Design. Research on the movement of the overlying strata in mining engineering has been a black box problem. Similarity material simulation tests provide an effective solution for studying overburden deformation and rock structure evolution during coal mining [31]. The similarity model was constructed using a 3000 × 200 × 2000 mm (length × width × height) plane stress model frame and based on the geological conditions of the Ningtiaota coal mine. The similarity model contained two coal seams that could be excavated. The thickness of the upper coal seam 1^{-2} was 1.95 m, and the thickness of its overburden was 123.05 m. The thickness of the lower coal seam 2^{-2} was 4.65 m, and the thickness of its overburden was 158.35 m. The inclination angle of the coal seam ranged from 1°47′ to 0°13′. The distance between the two coal seams was 33.35 m, i.e., short-distance coal seams. The similarity materials were composed of quartz sand, gypsum, and mica powder. These materials were mixed with ratios based on calculation results and the similarity theory [31] (Table 1). The geometric similarity ratio, bulk density similarity ratio, and stress similarity ratio were 1 : 150, 1 : 1.56, and 1 : 234, respectively.

The coal seam was excavated from the left side of the model to the rear side. One 30 cm wide boundary coal pillar

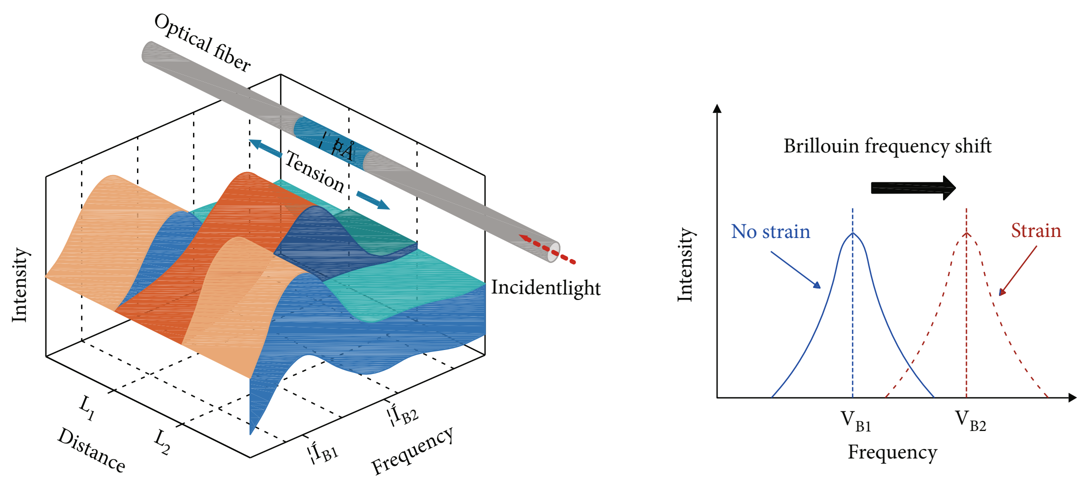

Figure 1: Monitoring principle of BOTDA.

Table 1: Material ratios used in the similarity material model.

Lithology of simulated stratum	Stratum thickness (m)	Simulated thickness (cm)	Accumulated height (cm)	Material ratio	Dosage of analogous materials (kg)		
					Sand	Gypsum	Mica powder
Loess	42.00	28.0	117.1	1019	238.25	2.38	21.44
Sandy mudstone	14.76	9.8	89.1	919	82.89	0.92	8.29
Siltstone	21.55	14.4	79.3	837	119.53	4.48	10.46
Medium-grained sandstone	28.75	19.2	64.9	837	159.47	5.98	13.95
Siltstone	6.70	4.5	45.8	937	37.63	1.25	2.93
Medium-grained sandstone	9.96	6.6	41.3	828	55.24	1.38	5.52
1^{-2} coal seam	1.89	1.3	34.7		5.13	0.19	1.28
Fine-grained sandstone	9.4	6.3	33.4	937	52.34	1.89	4.42
Siltstone	3.80	2.5	27.1	828	21.08	0.53	2.11
Fine-grained sandstone	5.90	3.9	24.6	837	32.73	1.23	2.86
Siltstone	1.00	0.7	20.7	937	5.62	0.19	0.44
Fine-grained sandstone	12.16	8.7	20.0	828	73.14	1.8	7.18
2^{-2} coal seam	4.60	3.1	11.2		12.48	0.47	3.12
Siltstone	3.54	2.4	8.2	937	19.88	0.66	1.55
Fine-grained sandstone	8.70	5.8	5.8	837	48.26	1.81	4.22

was left on each side of the model to eliminate the influence of the boundary effect on the similarity simulation test. In each coal seam, the excavation step was 3 cm, the number of excavations was 77, and the excavation length was 240 cm. Coal seam 1^{-2} was excavated first in the similarity simulation test. After the excavation, the model was allowed to settle for two weeks. After the overburden of the goaf behind the face was compacted, coal seam 2^{-2} was excavated.

2.3. Monitoring System Layout. The similarity simulation test monitoring system included a NX-6055 Brillouin scattering optical time-domain analyzer, distributed optical fiber sensors, CL-YB-114 pressure sensors, and a micrometer. The distributed optical fiber sensors (DOFSs) were common single-mode fibers with a diameter of 2 mm. The distributed optical fiber sensor layout is shown in Figure 2. Four vertically distributed optical fiber sensors (V1, V2, V3, and V4) were embedded in the similarity model to monitor the deformation characteristics of the overlying rocks. The spacing between the vertically distributed optical fiber sensors was 60 cm, and that between the horizontally distributed sensors was 39 cm. Each fiber sensor was connected in series with another fiber sensor and then connected with an NBX-6055 optical stress analyzer.

3. Analysis of Monitoring Results

Figure 3 shows the strain monitoring results of DOFS V1-V4 for the working-face mining of coal seam 1^{-2}. Figure 4 shows the strain monitoring results of the DOFS for the working-

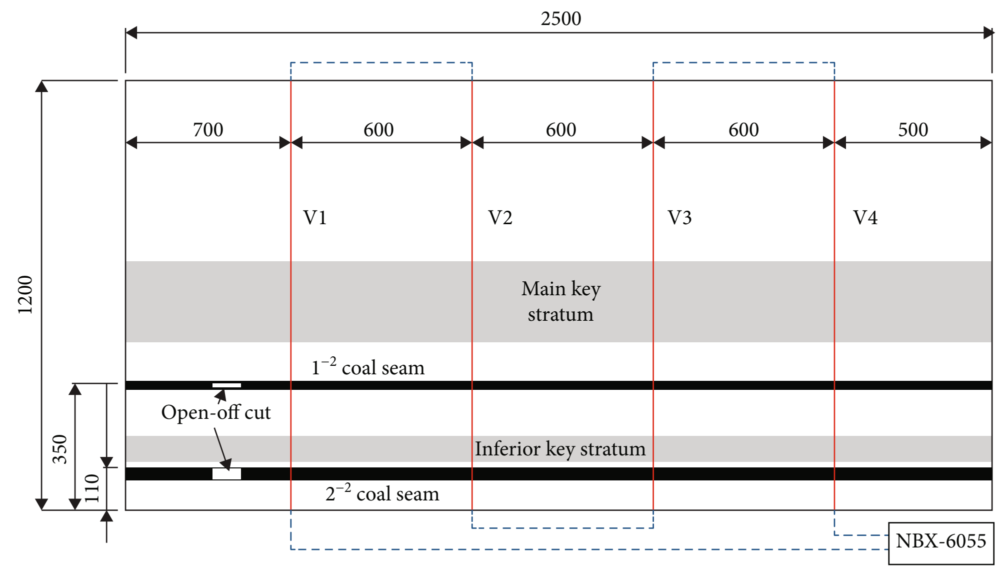

Figure 2: Layout of the distributed optical fiber sensors.

face mining of 2^{-2} coal seam. The vertical axis in Figures 3 and 4 represents the similarity model height, and the horizontal axis shows the strain monitoring value provided by the optical fiber. When the strain value is positive, the optical fiber is stretched. When the strain value is negative, the optical fiber is compressed.

When the optical fiber was far away from the face, the overlying rock containing the optical fiber was under the stress conditions of the original rock, and the strain value provided by the optical fiber was not affected by the mining. As the face was excavated, the strains of DOFSs V1-V4 were successively affected by the excavation. When the face was close to the rock in which the optical fiber was placed, the optical fiber reported negative growth with a small amplitude, and the strain peak occurred in the rock near the top of the coal seam. As the distance between the face and the optical fiber decreased, the strain peak value initially increased and then decreased. When the face reached and passed through the rock in which the optical fiber was placed, the strain peak value changed from negative to positive with a continuous increase. The strain peak value in the overburden also increased gradually and occurred in the middle and upper parts of the overburden. As the face moved far away from the optical fiber, the strain peak value decreased and then became stable. During the excavation of coal seams 1^{-2} and 2^{-2}, the strain monitoring curves of optical fibers V1-V4 exhibited clear trends in both their numerical values and structural forms as the face was excavated. Therefore, optical fiber strain monitoring can be used to invert the overburden failure characteristics during the mining process.

4. Analysis of Temporal and Spatial Distribution Characteristics of Overburden Strain

4.1. Analysis of Temporal and Spatial Evolutions of Overburden Strain. Figure 5 shows the strain distribution of optical fiber V3 during the mining of the face of coal seam 1^{-2}, with the vertical axis representing the similarity model height and the horizontal axis representing the distance between the face and V3. When the distance was negative, the face was close to the optical fiber. When the distance was positive, the face was far away from the optical fiber. The compression and tension regions are separated by the $0\,\mu\varepsilon$ curves. During the construction of the similarity model, a certain amount of prestress was applied to the distributed optical fiber sensors to make the distributed optical fiber sensors more sensitive to the changes in the overburden pressure during mining of the face. Therefore, before the face was mined, the lower part of the model in the height range of 0-53 cm was under slight compression, while the upper part of the model in the height range of 53-120 cm was under slight tension. As the face approached optical fiber V3, the compressive strain range of V3 increased due to the influence of the advanced support pressure. When the face was advanced to the position of V3, the compressive stress affected an expanded height range of 0-79 cm in the similarity model. The compressive strain provided by the optical fiber sensor near the face was the greatest, reaching $-452.29\,\mu\varepsilon$. After the face passed V3, tensile strain appeared in the overlying strata. As the face was excavated, the range of the tensile strain expanded, and the peak strain position moved upward. When the face had advanced to 42 cm past optical fiber V3, the peak tensile strain reached the maximum value of $7627.85\,\mu\varepsilon$, occurring in the overlying rock at a height of 51.0 cm above the face of coal seam 1^{-2}. As the face progressed farther away from V3, the fiber strain gradually changed from tensile to compressive, indicating that the overburden in the goaf was gradually compacted.

Figure 6 shows the strain distribution of V3 during the mining of coal seam 2^{-2}. After the face was excavated during the mining of coal seam 1^{-2}, the overburden gradually recovered to the stress level of the original rock. The bottom part of the similarity model (height range of 0-24 cm) was affected by the impact pressure. As the face approached

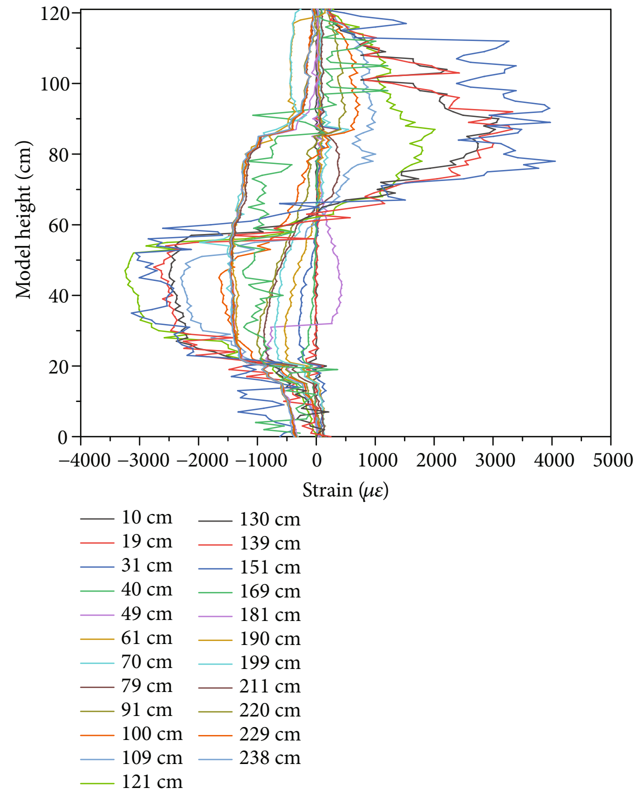

(a) DOFS V1

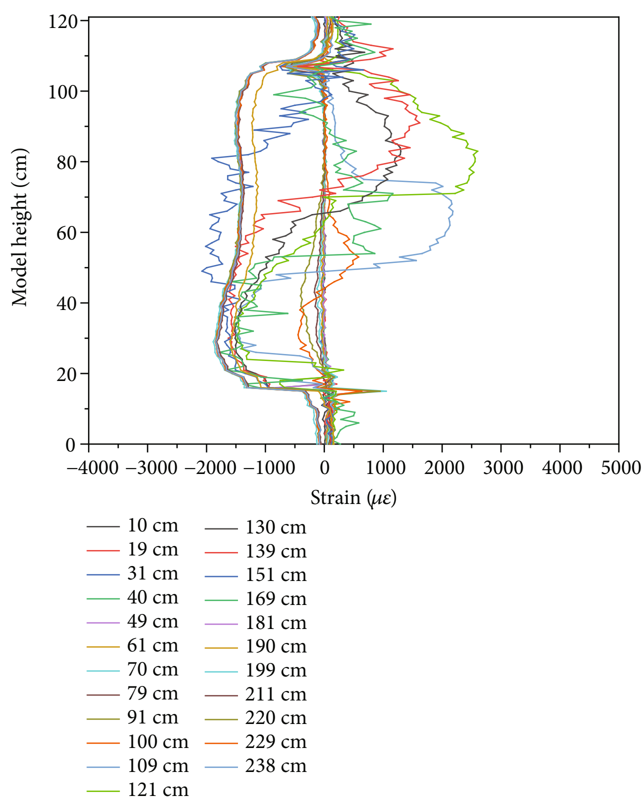

(b) DOFS V2

Figure 3: Continued.

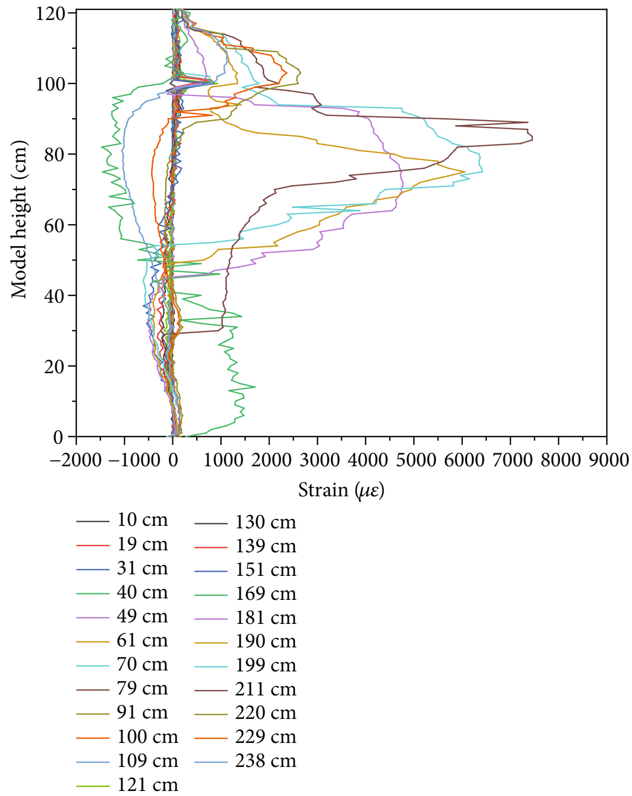

(c) DOFS V3

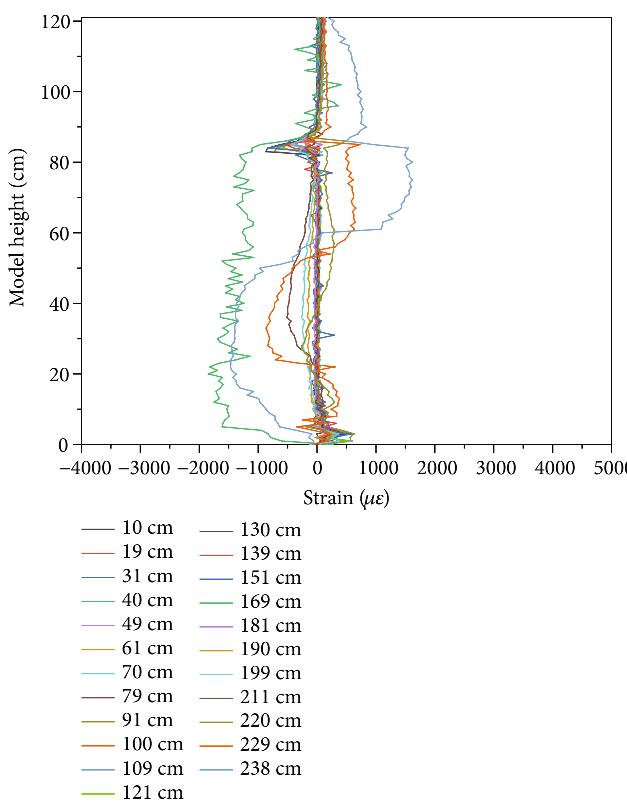

(d) DOFS V4

Figure 3: Strain monitoring results of DOFS V1-V4 in the mining of coal seam 1^{-2}.

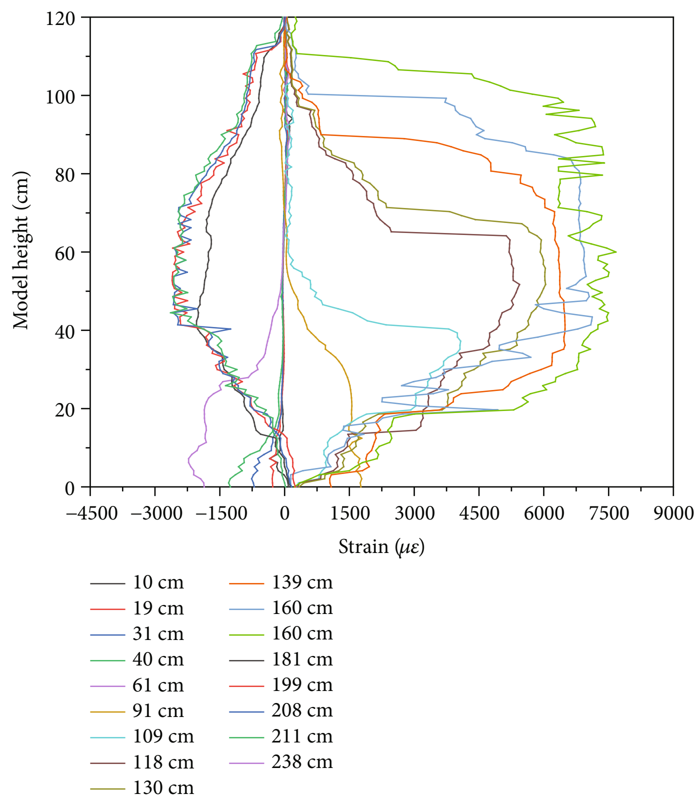

(a) DOFS V1

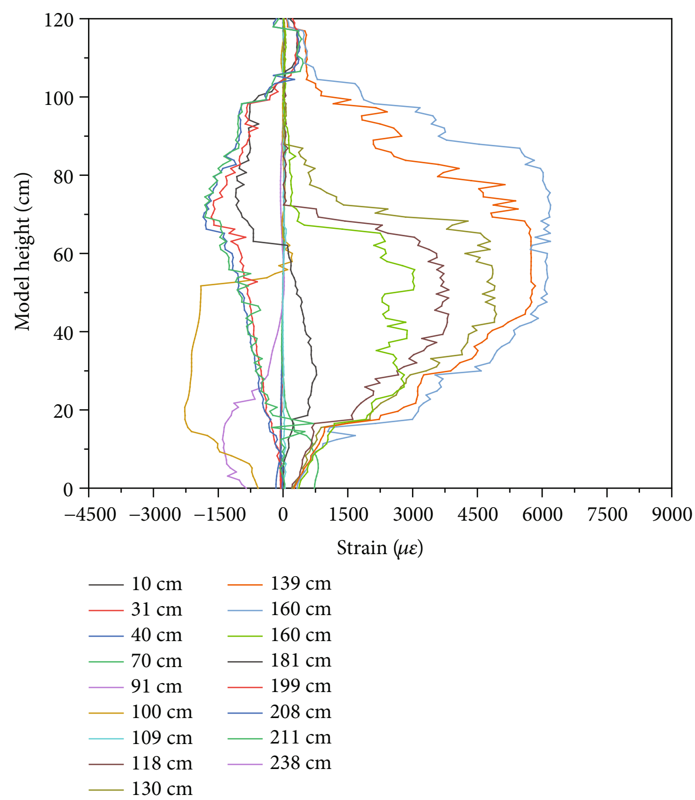

(b) DOFS V2

Figure 4: Continued.

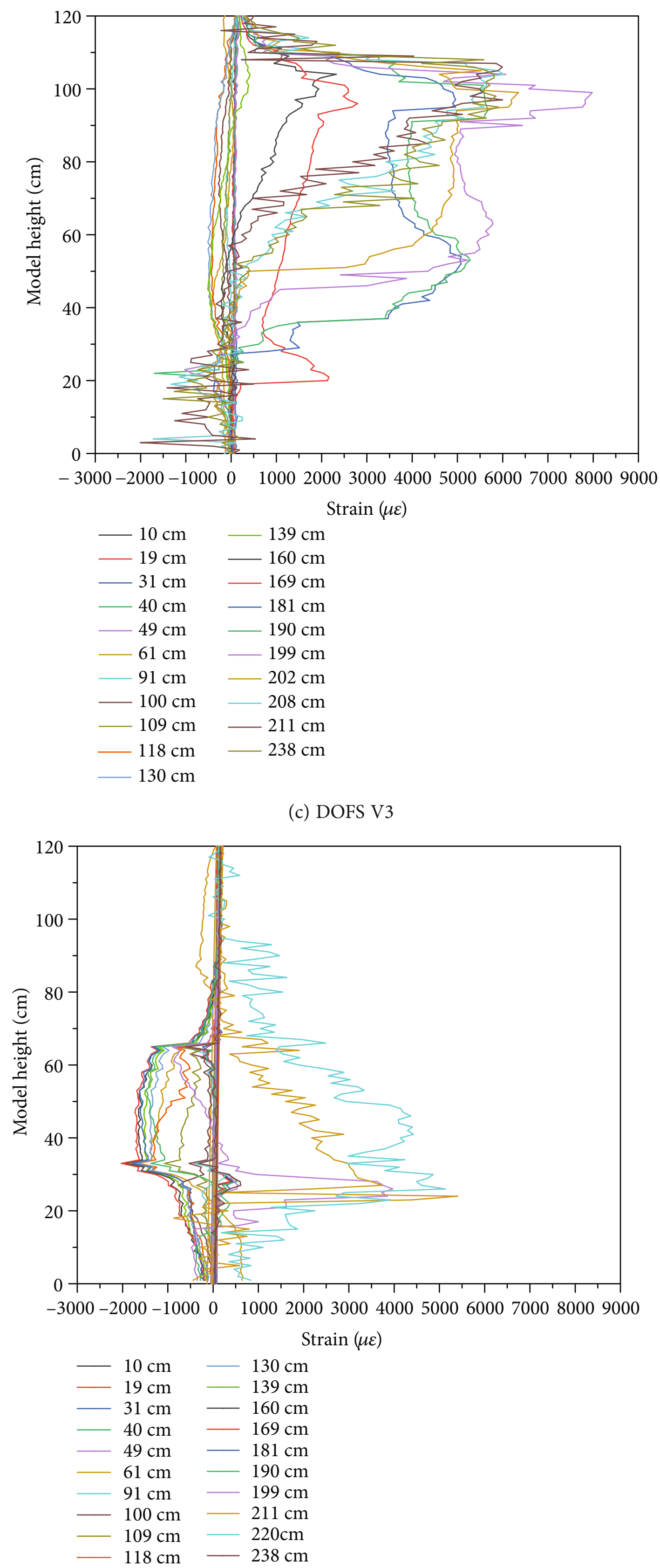

(c) DOFS V3

(d) DOFS V4

FIGURE 4: Strain monitoring results of DOFSs V1-V4 in the mining of coal seam 2^{-2}.

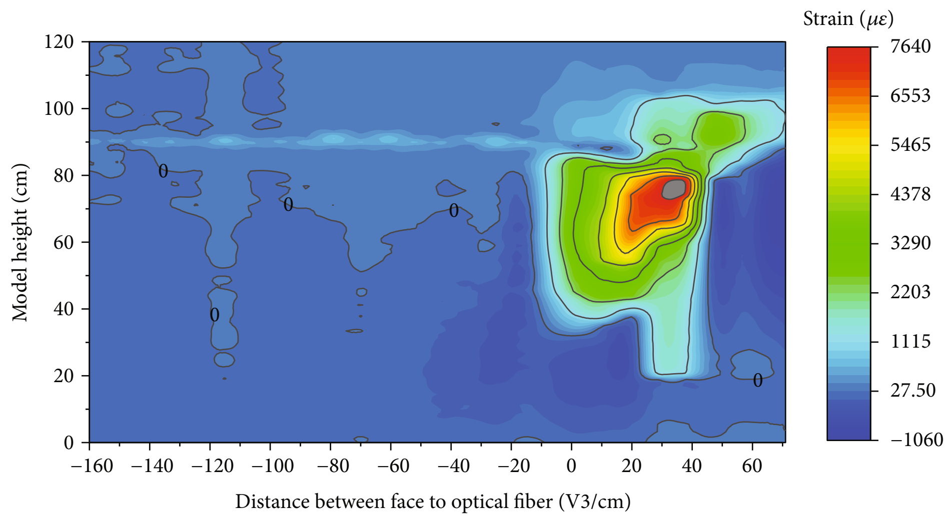

FIGURE 5: Strain distribution of fiber V3 during the mining of coal seam 1^{-2} (the abscissa is the model height, and the ordinate is the distance between the face and the optical fiber).

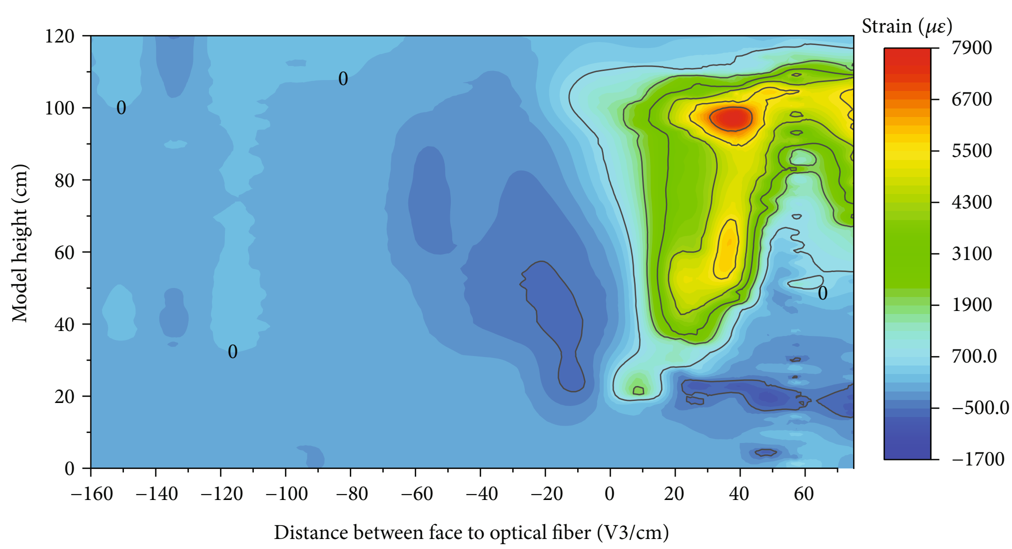

FIGURE 6: Strain distribution of fiber V3 during the mining of coal seam 2^{-2} (the abscissa is the model height, and the ordinate is the distance between the face and the optical fiber).

V3, the broken overburden rocks in the goaf of coal seam 1^{-2} did not have any capacity to sustain loads. Therefore, the rocks all caved downward into the goaf of coal seam 2^{-2} under the influence of the secondary mining, resulting in the compression range of the optical fiber gradually increasing. When the face was 21-58 cm away from V3, the compressive strain range of the overburden was the greatest, and the entire height range of 0-114 cm in the similarity model was under compressive strain. When the face passed through and progressed farther away from the position of V3, the deformation characteristics were similar to the deformation characteristics of the overlying strata during the excavation of coal seam 1^{-2}. When the face was 39 cm away from V3, both the range and peak value of the tensile strain reached their maxima, with a maximum tensile strain of 7867.18 $\mu\varepsilon$ and the position of the maximum tensile strain located at a height of 88 cm above the face of coal seam 2^{-2}.

4.2. Optical Fiber Monitoring Analysis of Overburden Damage. Figure 7 shows the fiber strain curves as the face successively approached, passed through, and progressed farther away from the fiber sensor. A direct relationship between the fiber strain curves and the overburden deformation characteristics was established under these different excavation conditions.

The strain monitoring curve for the case of the face approaching V1 is shown in Figure 7(a). When the face was excavated from 0 to 40 cm, it became gradually closer to the optical fiber. The optical fiber was in a coal wall support area of the face. Under the influence of the advance

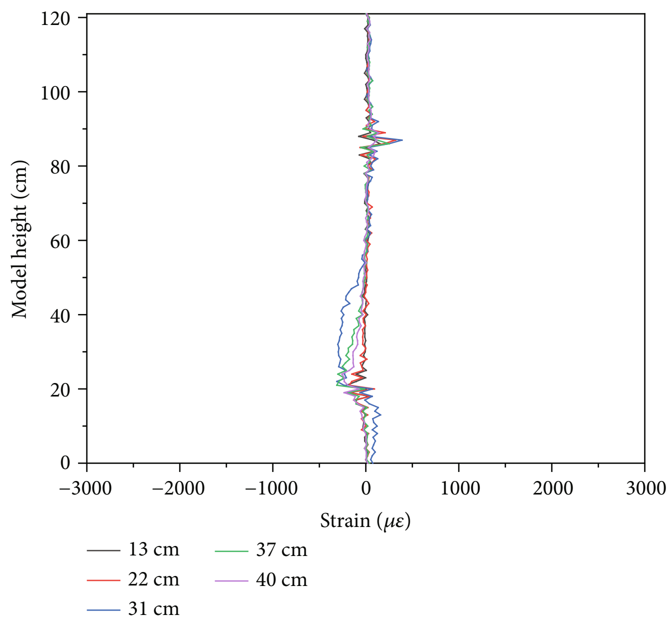

(a) Stage 1: the face is close to the optical fiber

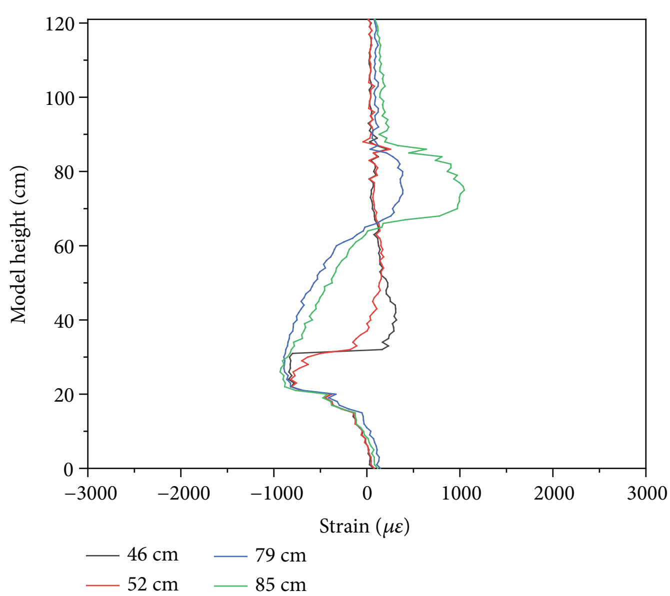

(b) Stage 2: the face passes the optical fiber

FIGURE 7: Continued.

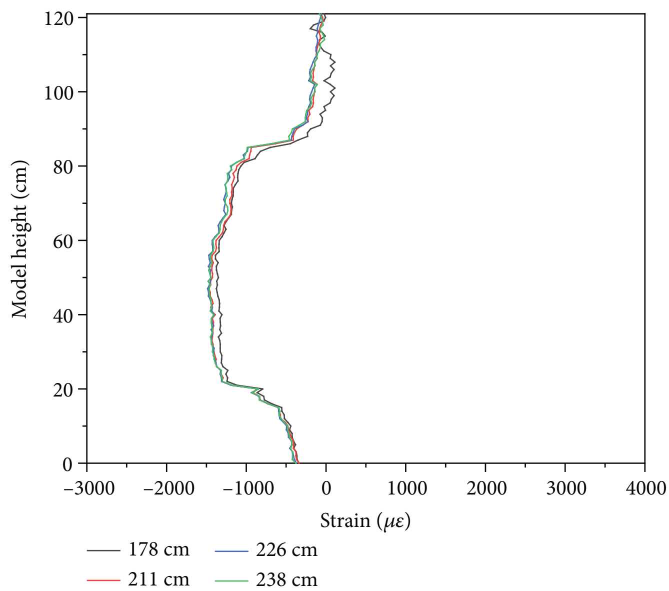

(c) Stage 3: the face is far away from the optical fiber

Figure 7: Strains of vertical fiber V1 at different positions relative to the face.

support pressure, compressive strain occurred in the lower part of the optical monitoring fiber. As the face advanced toward the optical fiber, the compressive strain initially increased and then decreased. The maximum compressive strain was $-295.52\,\mu\varepsilon$, and it occurred when the excavation advanced to 31 cm from V1. The variation trends of the optical fiber's compressive strain in front of the face verify the distribution characteristics of the advance support pressure in front of the face [5]. The position of the peak compressive strain was the same as the position of the maximum advanced support pressure in front of the face.

The strain monitoring curve for the case of the face passing through V1 is shown in Figure 7(b). When the face was excavated from 43 to 85 cm, the face passed through the optical fiber. When the face passed through the optical fiber by 0-12 cm, the optical fiber sustained tensile strain. As the face was excavated further, the fiber's strain curve exhibited a three-step distribution. The optical fiber's strain was negative in the height range of 0-31 cm above the face, corresponding to heights of 35-66 cm in the similarity model, and the compressive strain gradually increased. The fiber's strain was positive in the height range of approximately 31-52 cm above the face, corresponding to heights of 66-87 cm in the similarity model. According to the three-zone theory of the overburden [32], the step in the negative strain curve corresponded to the overburden fracture zone, where the fractured rocks were gradually compacted, causing a gradually increase in the compressive strain. The step in the positive strain curve corresponded to the overburden crack zone, where the optical fiber was strained. A bending subsidence zone was located above the crack zone. The fiber's strain decreased in the bending subsidence zone.

The strain monitoring results for the case of the face being far away from V1 are shown in Figure 7(c). When the face was excavated from 88 to 240 cm, the face was far away from the optical fiber. In this stage, because the face had been fully excavated, the overburden rocks collapsed in a large area and gradually and firmly pressed on the lower caving zone, eliminating the cracks in the middle crack zone and causing a negative strain in the optical fiber due to the overall compression effect. The upper part of the similarity model was a bending subsidence zone, in which the fiber's strain varied very little.

As the face progressed farther away from V1, the impact of the mining on optical fiber's signal became weak, while optical fibers V2, V3, and V4 were gradually influenced by the mining to a greater extent, and their strains' variation trends were similar to that of V1. These analysis results show that the peak position of the advanced support pressure on the face and the heights of the caving zone and fracture zone in the overburden goaf can be estimated based on the relative positions of the optical fiber and the face and on the optical fiber monitoring characteristic curves under different overburden deformation conditions.

5. Optical Fiber Monitoring Analysis of the Face Impact Pressure

5.1. Relationship between Face Impact Pressure and Optical Fiber Frequency Shift. When the coal seam was not excavated, the overlying rocks were not disturbed by mining, and the fiber's Brillouin frequency shift in the similarity model did not change. When the face was excavated, the large-scale collapse of the overlying strata caused the impact pressures to act on the face. The face impact pressure is of great importance to the safety of the face. The overburden collapse in a large area caused drastic variations in the fiber's Brillouin frequency shift in the similarity model. Therefore, the variation of the fiber frequency shift can be used to characterize the occurrence of the face impact pressure.

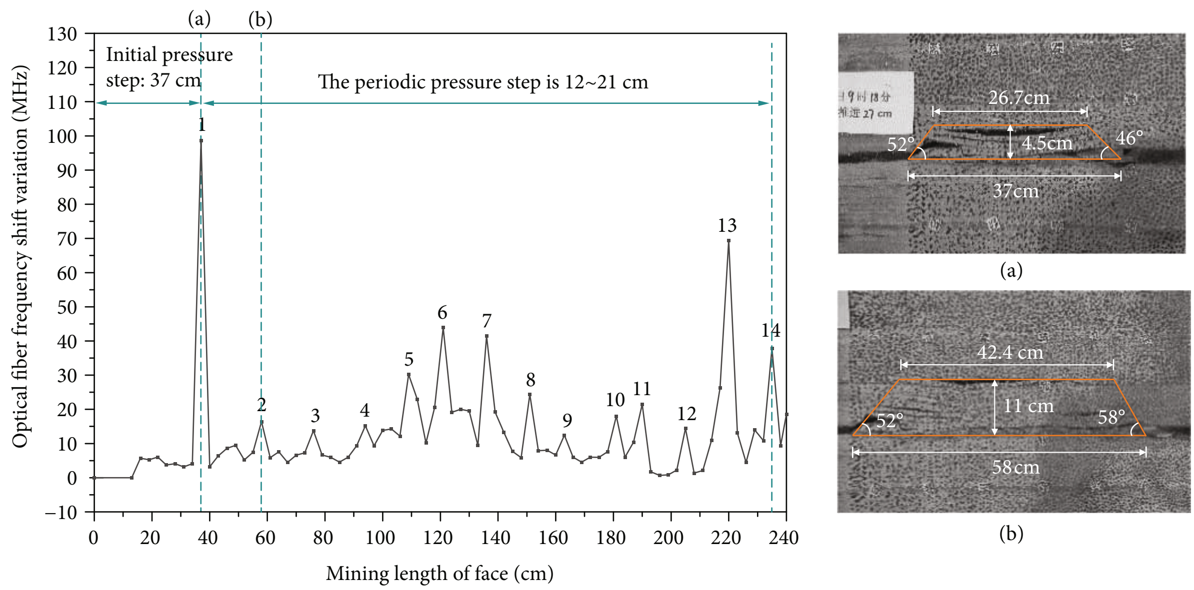

Figure 8: Impact pressure identification curves during the mining of coal seam 1^{-2} (the abscissa is the face excavation distance, and the ordinate is the variation degree of the optical fiber frequency shift). (a) Face excavation distance of 37 cm. (b) Face excavation distance of 58 cm.

The concept of the variation degree of the optical fiber frequency shift can be explained as follows. There are j collected samples of the frequency shift in the optical fiber monitoring database, and there are n sampling points for each data sample. The difference in the frequency shifts of two collected samples in a given space is normalized to characterize the deformation degree of the rock structure and to reflect the intensity of the rock movement. The variation degree is expressed as follows:

$$D_x = \frac{1}{n}\left(\sum_{j=1}^{n}\left|\mathrm{BFS}_j\right| - \sum_{j=1}^{n}\left|\mathrm{BFS}_{j-1}\right|\right), \quad (2)$$

where D_x is the variation degree of the optical fiber frequency shift in the testing when the face is excavated for a distance x, and n is the number of sampling points for the optical fiber. When the overburden strata experience small deformations, the frequency shift variation of the monitoring fiber is small. When the overburden strata experience a large separation or are even broken and fall, the frequency shift variation is large.

5.2. Characterization of Face Impact Pressure Based on Optical Fiber Frequency Shift Variation. During the face mining, the strata containing fibers V1-V4 were affected by the mining disturbances. Therefore, the variation degree of the optical fiber frequency shift throughout the entire process of mining the face was the sum of the variation degree of each optical fiber (V1, V2, V3, and V4) (Figures 8 and 9). The horizontal axis in the figures represents the mining distance of the face, and the vertical axis represents the variation degree of the optical fiber frequency shift.

Figure 8 shows that there were a total of 14 spikes in the optical fiber frequency shift curve during the mining of the face of coal seam 1^{-2}, indicating that there were 14 episodes in which the impact pressures acted on the face, corresponding to excavation distances of 37, 58, 76, 91, 109, 124, 136, 151, 163, 178, 190, 205, 220, and 235 cm. The first peak corresponded to the appearance of the first impact pressure when the face was excavated to 37 cm, with a frequency shift of 98.69 MHz, and the first impact pressure acted on the face. It occurred when the basic overburden roof overhang reached the span limit, shear fractures formed along the coal wall of the face under the effects of the rock weight and the pressure caused by the upper overburden rocks. The step distance, the mining length of the working face from the time of impact pressure to the time of last pressure, of the initial impact pressure was 37 cm. The height of the fracture zone was 4.5 cm. The overburden caving angle was 52° on the side farther away from the face. The overburden caving angle was 46° on the side closer to the face. Rock separation occurred above the basic overburden roof, and the maximum height of the stratum gap was 1 cm. The stratum gap gradually closed as the excavation continued. The overlying rocks located in the goaf were entered the pressure relief zone. The second peak in Figure 8 occurred when the face was excavated to 58 cm, with a frequency shift variation degree of 16.41 MHz, and the first periodic impact pressure occurred on the face. The broken rocks rotated unstably toward the goaf. The step distance of the first periodic impact pressure was 21 cm. After the second peak, multiple periodic impact pressures acted on the face. It can be observed that the step distances of the periodic impact pressures were 12-21 cm, with an average of 15.5 cm. The variation degrees of the optical fiber frequency shift were 12.44-98.69 MHz.

Figure 9 shows that there were 16 peaks in the variation degree curve of the optical fiber frequency shift for the face of coal seam 2^{-2} during the mining process, indicating that

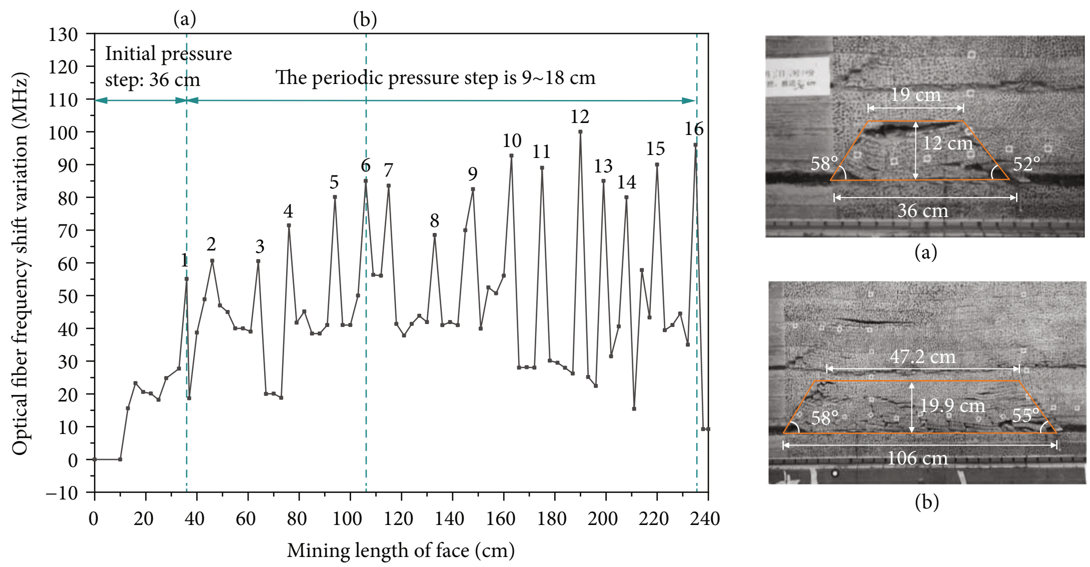

Figure 9: Impact pressure identification curve during the mining of the face of coal seam 2^{-2} (the abscissa is the face excavation distance, and the ordinate is the variation degree of the optical fiber frequency shift). (a) Face excavation distance of 36 cm. (b) Face excavation distance of 106 cm.

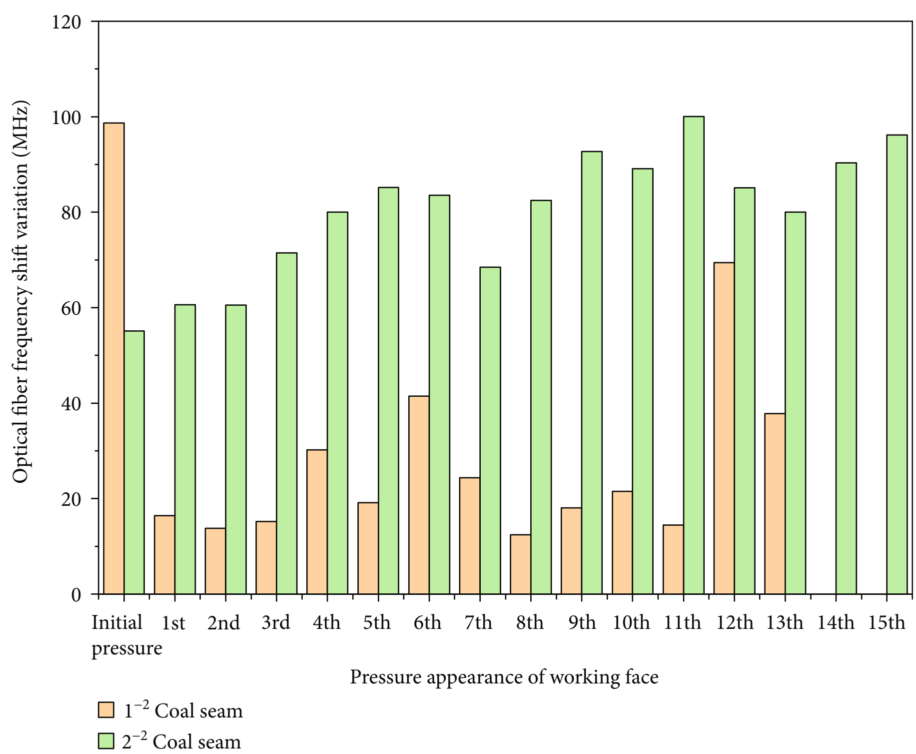

Figure 10: Comparison of the variation degree of the optical fiber frequency shift with the impact pressure (the ordinate is peak values in the mining of coal seams 1^{-2} and 2^{-2}).

the impact pressures acted on the face 16 times, including one initial impact pressure and 15 periodic pressures. The step distance of the initial impact pressure was 36 cm, while the step distances of the periodic pressures were 9-18 cm, with an average of 13.27 cm. The variation degrees of the frequency shift were 60.52-103.45 MHz. It can be seen that the step distances of the impact pressures in the mining of the lower coal seam were less than those in the mining of the upper coal seam in the short-distance coal mining.

5.3. Comparison of the Face Impact Pressure in Short-Distance Coal Seam Mining. The mining of lower coal seam 2^{-2} caused repeated disturbances to the stress of the overlying strata, resulting in the intensity of the impact pressures

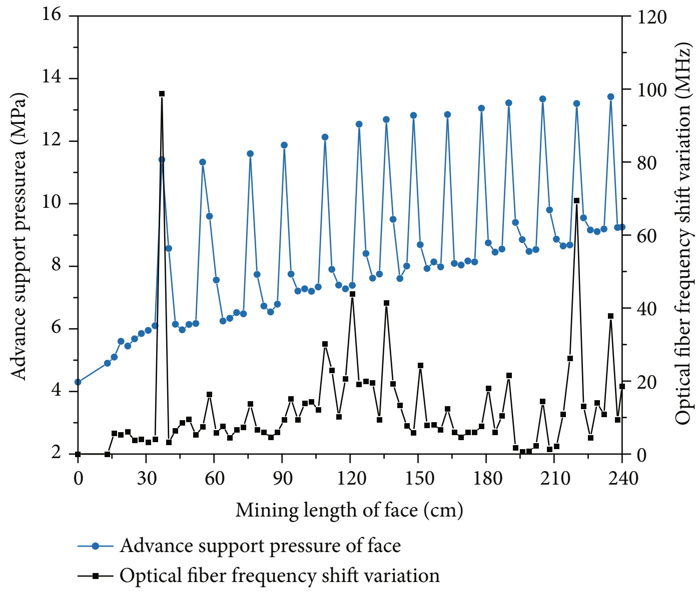

(a) Impact pressure acting on the face during the mining coal seam 1^{-2}

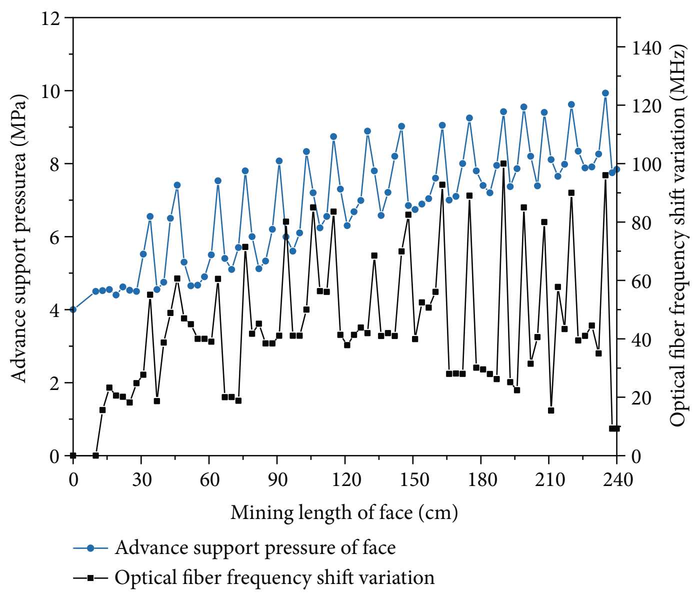

(b) Impact pressure acting on the face during the mining of coal seam 2^{-2}

Figure 11: Comparison of the impact pressures monitored by the optical fiber sensors and the pressure sensors.

acting on the face in the lower coal mining differing from that in the upper coal mining. Figure 10 shows the comparison of the variation degree of the optical fiber frequency shift in the impact pressure events on the face during the mining of coal seams 1^{-2} and 2^{-2}.

Figure 10 shows that the average variation degrees of the mining of coal seams 1^{-2} and 2^{-2} were 30.92 and 80.06 MHz, respectively, with a ratio of 1 : 2.64. This indicates that the average intensity of the impact pressures in the mining of coal seam 2^{-2} was 2.64 times that in the mining of coal seam 1^{-2}, reflecting the more violent mining environment of coal seam 2^{-2}. The reason for this phenomenon was that after the upper coal mining was completed, the overburden changed from intact rocks to broken rocks, and the caved rocks fell into the goaf. The load-sustaining capacity of the caved rocks was greatly reduced, causing its load to directly act on the coal seam floor in the goaf. When a single key layer in lower coal seam 2^{-2} overburden was broken during face mining, the caving of the overburden in the original goaf was affected by the secondary mining, causing overall clipped collapse and step subsidence of the overburden. This is the reason why the intensity of the impact pressures in this type of mining is greater than that in single-coal-seam mining. Moreover, the mining height of the lower coal seam was 2.38 times that of the upper coal seam. The higher mining height caused greater vertical deformation of the overburden. When the coal seam spacing was smaller, it was easier for the cracks in the overburden of the lower coal seam to penetrate into the goaf of the upper coal seam. Therefore, the impact pressures during the short-distance mining of the lower coal seam mining were more violent than those in single-coal-seam mining.

5.4. Comparative Analysis of Pressure Sensor Measurement Results. The pressure of the overlying strata during the coal mining process was measured using CL-YB-114 pressure sensors installed at the bottom of the similarity model. The coal seam excavation caused the advanced support pressure of the overburden, which was sustained by the coal wall in front of the face. When the impact pressure occurred, the peak value of the advanced support pressure increased rapidly. Therefore, the peak value of the monitored curve of the advanced support pressure can be used to judge whether an impact pressure event occurred.

For the mining of the faces of coal seams 1^{-2} and 2^{-2}, the comparisons of the variation degrees of the optical fiber frequency shifts and the peak values of the advanced support pressures provided by the pressure sensors are shown in Figure 11. The initial pressure of the overburden was measured by the pressure sensors before the face was excavated. The initial support pressure measured in coal seam mining 1^{-2} was 4.30 MPa, while that in coal seam 2^{-2} was 4.00 MPa. This is because the overburden pressure was reduced by the mining of coal seam 1^{-2}. The overburden pressure sustained by the coal wall increased gradually during the excavation of the face, and the peak values of the advanced support pressures also increased gradually. The curve of the pressure sensors exhibits continuous convex peaks. When the peaks occurred, the initial impact pressure or periodic pressures occurred on the face. During the mining of coal seams 1^{-2} and 2^{-2}, the pressure sensors detected 14 and 16 impact pressure events, respectively. Moreover, the step distances of the impact pressures detected by the pressure sensors were consistent with the signals reflected by the variation degree of the optical fiber frequency shift. Therefore, the frequency shift variation can be used to characterize the impact pressure acting on the face.

6. Conclusions

In this study, critical issues in applying distributed optical fiber sensing to monitoring overburden deformation using similarity simulation tests were investigated. The relationships between the optical fiber monitoring, overburden deformation, and face impact pressure were explored. The following conclusions were drawn.

(1) Overburden strain monitoring during the entire mining process was achieved at different relative positions between the distributed optical fiber sensors and the face. The peak positions of the advanced support pressures acting on the face were obtained. The three-step characteristics of the Brillouin frequency shift curve of the vertically distributed fiber sensors reflect the dynamic variation of the overburden movement in the goaf. They can quantitatively describe the height evolution characteristics of the overburden fracturing zone and the crack zone in the similarity model

(2) A new method was proposed for characterizing the impact pressure acting on the face based on the variation degree of the optical fiber frequency shift. The number of impact pressure events detected by the optical fiber frequency shift variation was basically consistent with the pressure sensor monitoring results, thus validating the proposed method

(3) The variation characteristics of the impact pressures acting on the face during short-distance coal mining were revealed by analyzing the characteristics of the optical fiber frequency shift variation curves. The step distances of the impact pressures during the mining of the lower coal seam were less than those during the mining of the upper coal seam, but the intensity of the impact pressures was greater than that during the mining of the upper coal seam

Data Availability

All the data, models, or codes that support the findings of this study are available from the corresponding author upon reasonable request.

Conflicts of Interest

The authors declare that they have no conflicts of interest.

Acknowledgments

We are grateful for financial support by the Key Program of the National Natural Science Foundation of China (Nos. 51804244, 41027002, and 52004203) and Scientific Research Project of Shaanxi Provincial Department of Education (16JK1488). Many thanks go to Professor J. Chai for the guidance in this paper. We would also like to thank Dr. Wang and Dr. Du for their valuable comments and suggestions for improving the manuscript.

References

[1] J. C. Wang, "Sustainable coal mining based on mining ground control," *J. Min. Strat. Control Eng.*, vol. 1, pp. 1–8, 2019.

[2] Q. Wang, M. He, S. Li et al., "Comparative study of model tests on automatically formed roadway and gob-side entry driving in deep coal mines," *International Journal of Mining Science and Technology*, vol. 31, no. 4, pp. 591–601, 2021.

[3] C. Zhu, K. Zhang, H. Cai et al., "Combined application of optical fibers and CRLD bolts to monitor deformation of a pit-in-pit foundation," *Advances in Civil Engineering*, vol. 2019, Article ID 2572034, 16 pages, 2019.

[4] W. Du, J. Chai, D. Zhang, and W. Lei, "The study of water-resistant key strata stability detected by optic fiber sensing in shallow-buried coal seam," *International Journal of Rock Mechanics and Mining Sciences*, vol. 141, p. 104604, 2021.

[5] P. S. Zhang and B. Sun, "Distribution characteristics of the advance abutment pressure in a deep stope," *Journal of Geophysics and Engineering*, 2020.

[6] T. Zhigang, Z. Chun, W. Yong, W. Jiamin, H. Manchao, and Z. Bo, "Research on stability of an open-pit mine dump with fiber optic monitoring," *Geofluids*, vol. 2018, Article ID 9631706, 20 pages, 2018.

[7] F. N. Wang, Z. B. Guo, X. B. Qiao et al., "Large deformation mechanism of thin-layered carbonaceous slate and energy coupling support technology of NPR anchor cable in Minxian Tunnel: a case study," *Tunnelling and Underground Space Technology*, vol. 117, p. 104151, 2021.

[8] X. Li, K. Peng, J. Peng, and H. Xu, "Effect of cyclic wetting-drying treatment on strength and failure behavior of two quartz-rich sandstones under direct shear," *Rock Mechanics and Rock Engineering*, 2021.

[9] F. Wu, H. Zhang, Q. Zou, C. Li, J. Chen, and R. Gao, "Visco-elastic-plastic damage creep model for salt rock based on fractional derivative theory," *Mechanics of Materials*, vol. 150, p. 103600, 2020.

[10] C. O. Aksoy, H. Kose, T. Onargan, Y. Koca, and K. Heasley, "Estimation of limit angle using laminated displacement discontinuity analysis in the Soma coal field, Western Turkey," *International Journal of Rock Mechanics and Mining Sciences*, vol. 41, no. 4, pp. 547–556, 2004.

[11] Q. Ye, G. Wang, Z. Jia, C. Zheng, and W. Wang, "Similarity simulation of mining-crack-evolution characteristics of overburden strata in deep coal mining with large dip," *Journal of Petroleum Science and Engineering*, vol. 165, pp. 477–487, 2018.

[12] J. Li, F. Li, M. Hu, X. Zhou, and Y. Huo, "Dynamic monitoring of the mining-induced fractured zone in overburden strata, based on geo-electrical characteristics," *Arabian Journal of Geosciences*, vol. 12, pp. 1–12, 2019.

[13] W. Zhou, P. Zhang, R. Wu, and X. Hu, "Dynamic monitoring the deformation and failure of extra-thick coal seam floor in deep mining," *Journal of Applied Geophysics*, vol. 163, pp. 132–138, 2019.

[14] D. D. Zhang, C. Ma, Y. Duan, W. du, J. Liu, and J. Chai, "Wavelength characteristic analysis of a FBG array embedded in quaternary unconsolidated strata during a deep borehole installation," *Journal of Sensors*, vol. 2021, Article ID 1207374, 13 pages, 2021.

[15] F. N. Wang, S. Yin, A. Guo et al., "Frame structure and engineering applications of the multisource system cloud service platform of monitoring of the soft rock tunnel," *Geofluids*, vol. 2021, Article ID 6672732, 15 pages, 2021.

[16] L. J. Butler, N. Gibbons, P. He, C. Middleton, and M. Z. E. B. Elshafie, "Evaluating the early-age behaviour of full-scale prestressed concrete beams using distributed and discrete fibre optic sensors," *Construction and Building Materials*, vol. 126, pp. 894–912, 2016.

[17] C. Pandian, M. Kasinathan, S. Sosamma et al., "Single-fiber grid for improved spatial resolution in distributed fiber optic sensor," *Optics Letters*, vol. 35, no. 10, pp. 1677–1679, 2010.

[18] W. Zou, Z. He, and K. Hotate, "Single-end-access correlation-domain distributed fiber-optic sensor based on stimulated Brillouin scattering," *Optics Index*, vol. 28, no. 18, pp. 2736–2742, 2010.

[19] T. Horiguchi, T. Kurashima, and M. Tateda, "Tensile strain dependence of Brillouin frequency shift in silica optical fibers," *IEEE Photonics Technology Letters*, vol. 1, no. 5, pp. 107-108, 1989.

[20] Y. Li, X. Y. Bao, Y. Dong, and L. Chen, "A novel distributed Brillouin sensor based on optical differential parametric amplification," *Journal of Lightwave Technology*, vol. 28, no. 18, pp. 2621–2626, 2010.

[21] K. Kishida, C. H. Li, and K. Nishiguchi, "Pulse pre-pump method for cm-order spatial resolution of BOTDA," in *17th International Conference on Optical Fibre Sensors*, pp. 559–562, Bruges, Belgium, May 2005.

[22] Kwang Yong Song, Sanghoon Chin, N. Primerov, and L. Thevenaz, "Time-domain distributed fiber sensor with 1 cm spatial resolution based on Brillouin dynamic grating," *Journal of Lightwave Technology*, vol. 28, no. 14, pp. 2062–2067, 2010.

[23] W. Du, J. Chai, D. Zhang, and W. Lei, "Application of optical fiber sensing technology in similar model test of shallow-buried and thick coal seam mining," *Measurement*, vol. 181, p. 109559, 2021.

[24] A. Klar and R. Linker, "Feasibility study of automated detection of tunnel excavation by Brillouin optical time domain reflectometry," *Tunnelling and Underground Space Technology*, vol. 25, no. 5, pp. 575–586, 2010.

[25] R. A. Moffat, J. F. Beltran, and R. Herrera, "Applications of BOTDR fiber optics to the monitoring of underground structures," *Geo-mechanics and Engineering*, vol. 9, no. 3, pp. 397–414, 2015.

[26] E. Buchoud, V. Vrabie, J. I. Mars et al., "Quantification of submillimeter displacements by distributed optical fiber sensors," *IEEE Transactions on Instrumentation and Measurement*, vol. 65, no. 2, pp. 413–422, 2016.

[27] D. Zhang, J. Wang, P. Zhang, and B. Shi, "Internal strain monitoring for coal mining similarity model based on distributed fiber optical sensing," *Measurement*, vol. 97, pp. 234–241, 2017.

[28] J. Chai, W. du, Q. Yuan, and D. Zhang, "Analysis of test method for physical model test of mining based on optical fiber sensing technology detection," *Optical Fiber Technology*, vol. 48, pp. 84–94, 2019.

[29] D. D. Zhang, Y. Duan, W. du, and J. Chai, "Experimental study on physical similar model of fault activation law based on distributed optical fiber monitoring," *Shock and Vibration*, vol. 2021, Article ID 4846977, 11 pages, 2021.

[30] D. D. Zhang, W. du, J. Chai, and W. Lei, "Strain test performance of Brillouin optical time domain analysis and fiber Bragg grating based on calibration test," *Sensors and Materials*, vol. 33, no. 4, pp. 1387–1404, 2021.

[31] Q. Yuan, J. Chai, Y. Ren, and Y. Liu, "The characterization pattern of overburden deformation with distributed optical fiber sensing: an analogue model test and extensional analysis," *Sensors*, vol. 20, no. 24, p. 7215, 2020.

[32] M. G. Qian and J. Xu, "Behaviors of strata movement in coal mining," *Journal of China Coal Society*, vol. 44, pp. 973–984, 2019.